Materials Research. 2022; 25(suppl. 2): e20220157
DOI: https://doi.org/10.1590/1980-5373-MR-2022-0157

Sustainable Carbon Xerogel in the Production of Electromagnetic Radar Absorbing Composites in the Ku-Band

***Nila Cecília de Faria Lopes Medeiros*[a,b*], *Leonardo Iusuti de Medeiros*[a,b], *Guilherme Frederico Bernardo Lenz e Silva*[c], *Alan Fernando Ney Boss*[c], *Newton Adriano dos Santos Gomes*[a], *André Ferreira Sardinha*[a], *Maurício Ribeiro Baldan*[a], *Gisele Amaral-Labat*[a]**

[a]*Instituto Nacional de Pesquisas Espaciais, Avenida dos Astronautas, 1758, 12227010, São José dos Campos, SP, Brasil.*
[b]*Universidade Estadual de Santa Cruz, Departamento de Ciências Exatas e Tecnológicas - DCET, Rodovia Jorge Amado, km16, 45662900, Ilhéus, BA, Brasil.*
[c]*Universidade de São Paulo, Departamento de Engenharia Metalúrgica e de Materiais, Avenida Professor Mello Moraes, 2463, 05508030, São Paulo, SP, Brasil.*

Received: March 24, 2022; Revised: June 29, 2022; Accepted: July 22, 2022

Carbonaceous porous materials are strong candidates for producing low-cost, lightweight, and sustainable electromagnetic (EM) absorbing materials. This work investigates the production of radar-absorbing materials (RAM) by a simple method. Sustainable carbon xerogel (CX) was synthesized from tannin, a biosourced molecule. CX and commercial carbon nanotube (CNT) were embedded in a silicone matrix at proportions of 10 and 15 wt.% of CX and 0.1 wt.% of CNT to produce flexible composites. The morphology and structure of the carbonaceous materials were evaluated by field-emission scanning electron microscopy (FEG-SEM), Raman spectroscopy, X-ray diffraction (XRD), textural properties by N_2 adsorption-desorption isotherms, and mercury porosimetry. The electromagnetic characterization of the composites was analyzed by a vector network analyzer (VNA) in the Ku-band. The results demonstrated that an increased concentration of CX in the composite improved reflection loss reaching -43.19 dB at 13.79 GHz.

Keywords: *Carbon Xerogel, Carbon Nanotube, Sustainability, Reflectivity, RAM.*

1. Introduction

Recently the rapid development of technologies for electronic devices has increased the electromagnetic pollution[1-3] promoting a growing research interest in developing new radar-absorbing materials (RAM)[2]. However, producing materials with suitable properties such as low density, great absorbing properties, and low cost is still a challenge[1,2]. At the same time, there is an increasing stimulation worldwide to produce sustainable materials due to the natural resource scarcity, climate change, and global warming as addressed by COP 26[4].

Tannin is a natural phenolic extracted from plants, which is cheaper than synthetic phenolic molecules and is a biosource widely employed to produce resins[5], foams[6], and gels[7], providing a sustainable approach to preparing green materials[8]. Organic biobased gels are synthesized from polymeric reactions, based on a sol-gel process from the tannin-formaldehyde system[9,10]. The polymerization reaction is performed between the natural phenolic precursor (tannin) and the crosslinker (formaldehyde) in an aqueous solution. The gelation process happens when the formed polymeric chains grow to form a macromolecule, becoming insoluble. The final product, called aquagel is composed of solid, spherical interconnected nodules enclosed by a large porosity filled with water and by-products[7]. Drying is a critical step because the liquid should be removed without generating surface tension, thus avoiding shrinkage and loss of porosity[7,11]. The evaporation of the liquid phase at room conditions (subcritical drying) generates a highly porous material named xerogel[11,12]. In this work, the surfactant F-127 Pluronic was applied to reduce the effects of surface tension during subcritical drying. This technique is the simplest and cheaper compared to supercritical drying and freeze-drying methods, which produce aerogel and cryogel, respectively[12]. For these drying methods, solvent exchange is mandatory, and reactors for supercritical conditions or freeze-dryers are needed, increasing the production costs. Furthermore, tannin is a natural phenolic, which is price-competitive compared to synthetic sources. Tannin is about 39 and 86 times cheaper than resorcinol and phenol, respectively[13]. Therefore, the synthesis of sustainable xerogels is a straightforward process with a high potential for large-scale production, and the pyrolysis of such materials provides a highly porous carbon with the desired properties

*e-mail: ncflmedeiros@uesc.br

for RAM, for example, low specific mass and cost along with a sustainable feature[11,14].

Several types of porous carbon nanomaterials have been explored as RAM[15,16], such as graphene[17-19], carbon nanotubes[20,21], metal-organic framework[22,23], and highly-oriented pyrolytic graphite[24], especially due to their physicochemical properties[25], in particular, the lightweight, high porosity, and electrical conductivity[21,26]; however, the complex preparation steps increase the final cost of such materials[16,23,27]. Accordingly, the use of a low-cost, sustainable carbon material might represent a promising alternative in the production of new RAMs. Furthermore, few works present the electromagnetic characterization of carbon xerogels[14,28]. Thus, a substantial lack of information concerning such materials in this field is clear. Most works on this topic apply carbon foams as RAM[29-32] at several frequencies including the X-band (8–12.4 GHz) and the Ka-Band (27–40 GHz). Additionally, electromagnetic characterization of biosourced materials is also scarce in the frequency range of 12.4–18 (Ku-Band), usually applied to aircraft and aerospace applications, such as radar, high-performance aircraft, and coatings for satellite by preventing electromagnetic interference, among other applications[33-38]. Therefore, the application of carbonaceous materials as a renewable resource in the aerospace sector could constitute an initial step toward developing sustainable technological advances in this field.

This work uses a sustainable carbon xerogel (CX) as a RAM filler and measures it in the frequency range of the Ku-band (12.4–18 GHz). Carbon nanotube (CNT) was added later to increase conductivity. The synthesis as well as the morphological and structural characterization of sustainable CX was performed.

2. Materials and Methods

2.1. Materials

Tannin powder (natural extract from *Acacia mearnsii* tree bark, kindly supplied by the company Tanac SA), ethyl alcohol (95%), Pluronic F-127 surfactant (Sigma), formaldehyde 37 wt.%, commercial multiwalled carbon nanotube with a diameter of 20–30 nm, 95 wt.% purity, length of 10–30 µm (Cheap Tubes) and white silicone rubber PS with high flexibility vulcanized elastomer a room temperature with hardness after cure 9–10 Shore (Redelease).

2.2. Methods

The gel was prepared by a simple polycondensation route in a sol-gel process[11]. The Pluronic F-127 surfactant (1.5 g) was dissolved in 18 g of deionized water: ethyl alcohol (1:1). Then 3 g of tannin powder and 6 g of formaldehyde were added under magnetic stirring until a homogeneous solution was obtained. The solution was transferred to a sealed reagent bottle and kept in an oven at 85 °C for five days for polymerization and for five more days at room condition to dry completely. The material was carbonized in a tubular oven at 900 °C for 120 minutes under nitrogen flow to produce the CX. The full production process of CX is shown in Figure 1.

The composite samples were made with silicone rubber and 10 wt.% CX, 15 wt.% CX, 10 wt.% CX + 0.1 wt.% CNT, and 15 wt.% CX + 0.1 wt.% CNT. All fillers were mechanically stirred for 5 minutes, and the mixtures were poured into molds with dimensions of 15.80 x 7.95 mm and thicknesses ranging from 2 to 6 mm, producing flexible sustainable composites, as shown in Figure 2. The maximum filler concentration (15 wt.% CX) was defined as the saturation

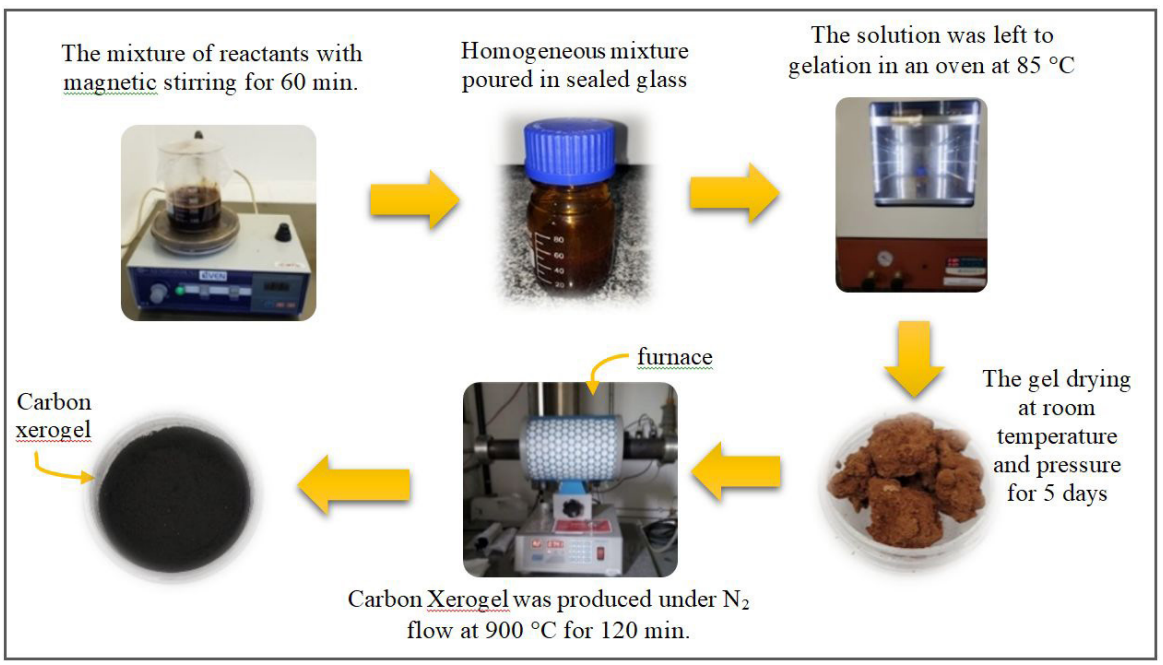

Figure 1. Production of the carbon xerogel.

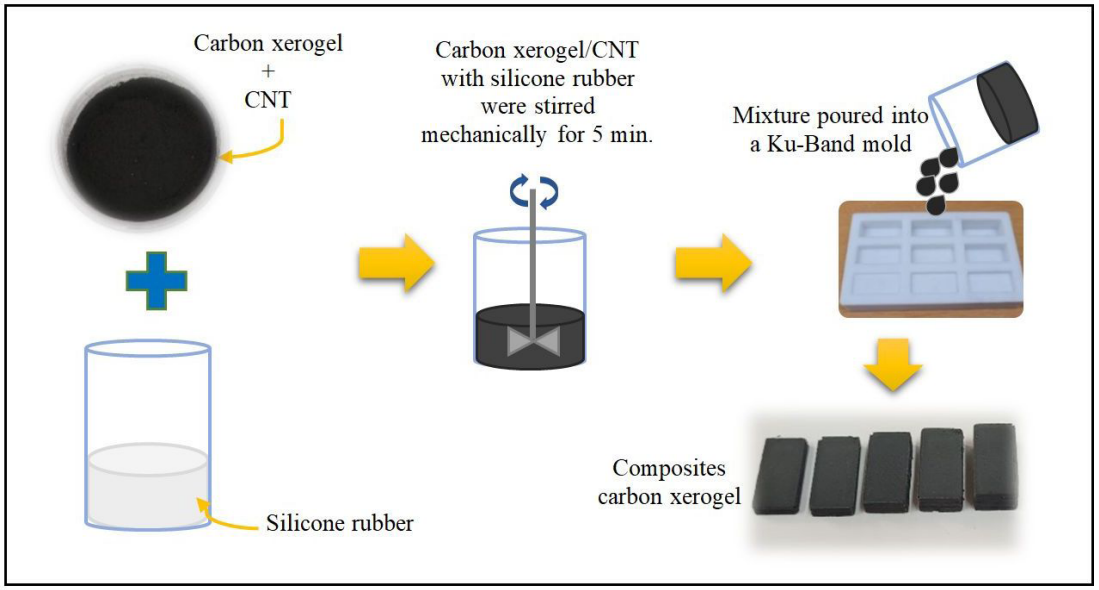

Figure 2. Production process of composites samples.

point. Concentrations greater than 15 wt.% of the CX did not allow the silicone rubber to cure. Pure CX composites were named accordingly to their concentrations of 10CX and 15CX. Samples containing carbon nanotube were named 10CX/0.1CNT and 15CX/0.1CNT.

The morphology of CX and CNT particles was evaluated through field-emission gun scanning electron microscopy (FEG-SEM; Mira3-Tescan). The graphitization was analyzed through Raman spectroscopy (Horiba-LabRam HR Evolution) using a green laser with a wavelength of 514.5 nm. The X-Ray diffraction (XRD) patterns were performed in a Rigaku diffractometer Ultima IV, using Cu Kα radiation (λ=0.15418 nm). The surface areas and the micropore volume of the CX and CNT samples were determined using the Brunauer-Emmet-Teller (BET)[39] and Dubinin-Radushkevic[40] methods from N_2 adsorption/desorption isotherms at -196 °C using a Micromeritics ASAP 2020 Plus for samples previously degassed for 24 hours at 200 °C. Additionally, the porous texture of CX was also performed by mercury porosimetry intrusion-extrusion curves (0.0035 MPa to 414 MPa) using the Micromeritics Instrument Corp, AutoPore III. The electromagnetic properties of the composite were evaluated by a vector network analyzer (VNA; N5235A *Keysight Technologies*), using a Ku-Band (12.4-18 GHz) rectangular cross-section waveguide kit (P11644A). The dielectric properties ($\varepsilon=\varepsilon'-j\varepsilon''$)[14,33,41] were obtained using the Nicolson-Ross-Weir (NRW) method, while the reflectivity was measured by the VNA using a metallic plate, as already explained elsewhere[42].

3. Results and Discussion

3.1. Morphological, chemical, and textural properties

The morphology of sustainable CX and the commercial CNT was evaluated by SEM images. Figure 3a, 3b shows a tridimensional chain with interconnected and spherical nodules in a microscale range average diameter of 25 μm, typical of tannin-formaldehyde xerogels[7,11,14]. Furthermore, a large porosity between the chains, ranging from 5–10 μm is clearly seen in Figure 3b. Figure 3c presents a cylindrical structure of entangled CNT[43] without preferential orientation with the average diameter of around 22 nm.

The graphitization degree of carbon raw materials, CX and CNT, was evaluated by Raman spectra (Figure 4). The CX shows the D and G bands at 1344 cm^{-1} and 1590 cm^{-1}, while the CNT shows these bands at 1350 cm^{-1} and 1575 cm^{-1}, respectively. Another peak in the carbon nanotube spectra refers to the G' band at 2700 cm^{-1}.

The D originates from structural defects. The presence of this band is observed even in very low-disordered carbon. The D band in nanotubes originates from tube wall defects. The presence of vacancies and dislocations in the graphene layer is a source of defects in carbon materials[44]. The G bands correspond to the sp^2 carbon networks plane in the two-dimensional hexagonal lattice[1,43,45]. The G' band is related to the vibrational mode originating from the second-order Raman scattering process of double resonance involving the two-phonon scattering mechanism[46-48]. The second order of D band, the G' band, is very sensitive to the stacking order of graphene sheets along the c axis[49].

The graphitization degree of carbonaceous materials is estimated by the intensity ratio of D and G bands (I_D/I_G)[1]. Figure 4 shows the I_D/I_G ratios of 0.65 and 1.03 for CNT and CX, respectively. These results show a higher crystalline structure of CNT compared to the amorphous structure of CX.

The XRD patterns of CX reveal peaks at 23.3° and 43.5°, while the CNT showed the same peaks at 26.1° and 43.1°, besides an additional peak at 53.65° (Figure 5). The first two peaks can be attributed to reflection planes (002) and (100) and the latter to (004), typical of the graphitic structure of carbonaceous materials[50-55].

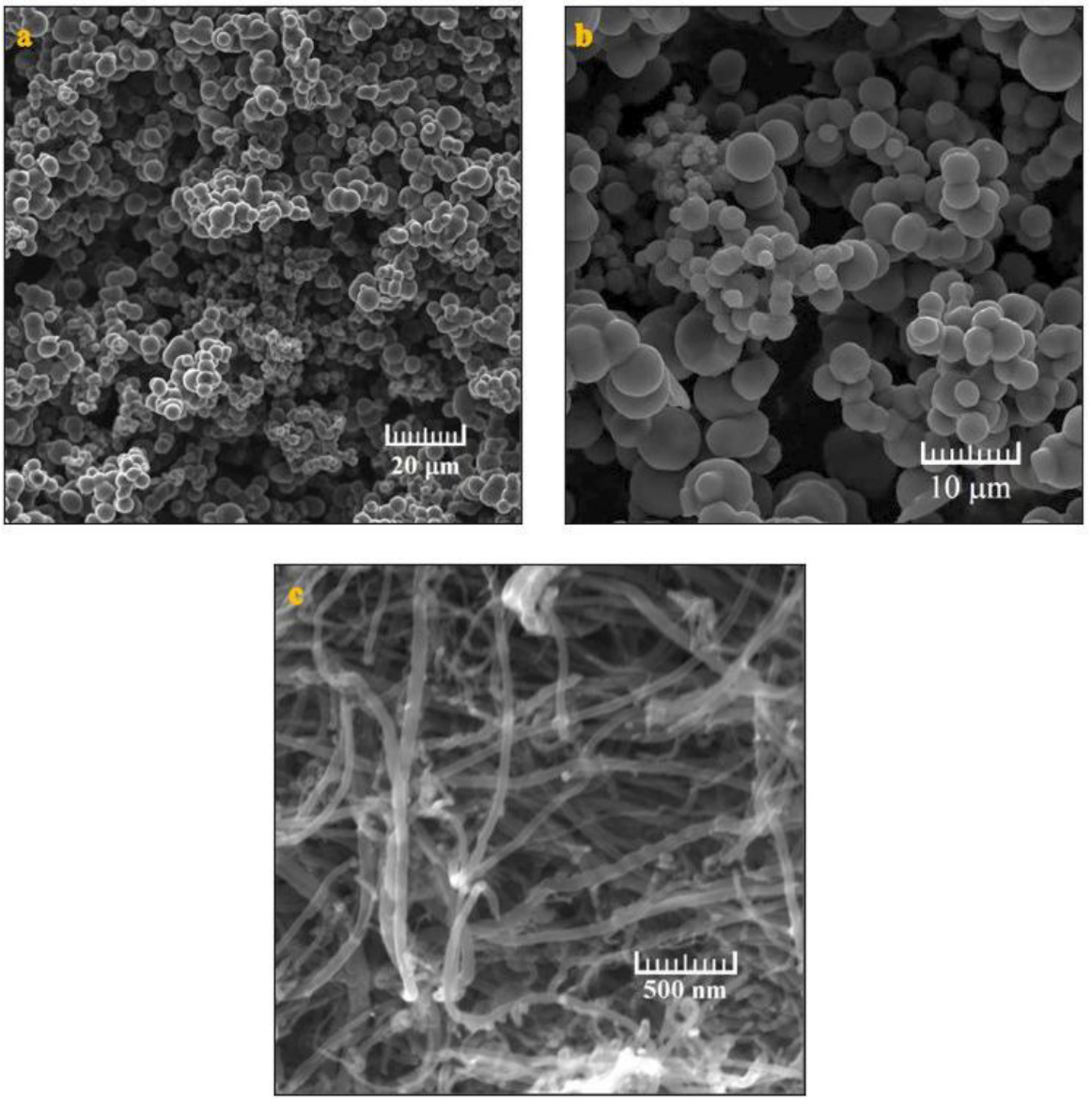

Figure 3. SEM images of: (a-b) CX (c) CNT.

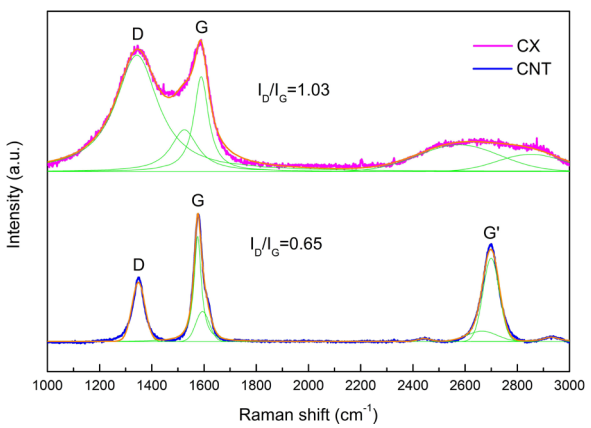

Figure 4. CX and CNT Raman spectra.

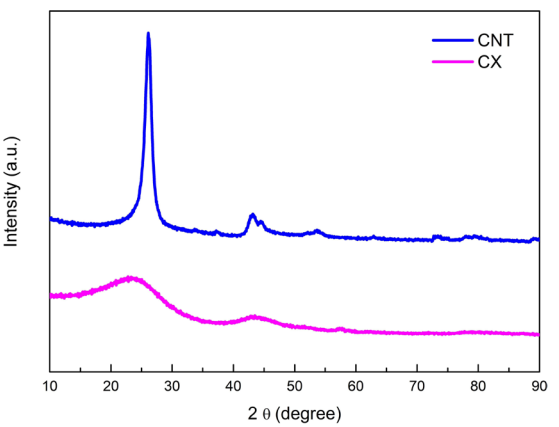

Figure 5. X-Ray Diffractogram of CX and CNT.

The nitrogen adsorption-desorption isotherms were performed for CX and CNT samples (Figure 6). The CNT demonstrated a combination of isotherms types I and IV, typical of micro-mesopores materials[56] while the CX showed no significant N_2 adsorption. The H2-hysteresis loop of the CNT sample is signed to percolation in a narrow range of pores neck[57].

The BET surface areas of CNT and CX were calculated from N_2 adsorption isotherms (Table 1), and the respective values are 90 $m^2.g^{-1}$ and 3 $m^2.g^{-1}$. The porosity of carbon materials is classified according to the pore width (d_{pore}): $d_{pore} < 2$ nm (micropores), $2 < d_{pore} < 50$ (mesopores) and $d_{pore} > 50$ nm (macropores)[58]. Therefore, the CNT presents a large mesoporosity and a moderate proportion of micropores (14%), while the CX showed no pores in the micro-mesoporosity range. Therefore, the porosity of CX is mainly composed of macropores (pores greater than 50 nm).

Figure 7 shows the pore-size distribution of CNT from the Barrett-Joyner Halenda (BJH) model[59]. The distribution presents a narrow peak centered at 2.6 nm related to the small pores on the cylinder surface[60] and a broad pore size distribution from 5–45, with a centered peak at 22.3 nm, probably related to the hollow cylinders, corroborated by the average diameter (22 nm) found by the SEM images.

The textural properties (Table 2) and macropore size distribution of the CX were evaluated by mercury porosimetry analysis (Figure 8). The bio-based CX synthesized at a mass fraction of 11 wt.% showed a low-density value comparable to carbon aerogels from tannin-formaldehyde at a mass fraction from 26–34 wt.% and pHs between 4–6[9]. The significant porosity (52%) and the respective total pore area might serve as a pathway for the electromagnetic wave acting as an attenuating material.

Figure 8 shows the mercury intrusion-extrusion curves obtained from the macroporous sustainable CX material. The hysteresis is attributed to the mercury trapped within the pores, as already observed for tannin-based gels[11,12] (Figure 8a). The pore size distribution (Figure 8b) shows peaks centered at 4 µm and 10 µm, agreeing with the SEM images, where voids in this scale range are clearly observed (Figure 3b).

3.2. Electromagnetic characterizations

The dielectric properties and reflectivity (RL) results of flexible composites from CX and CNT were evaluated by VNA. The complex permittivity of all samples 10CX, 15CX, 10CX/0.1CNT, and 15CX/0.1CNT are illustrated in Figure 9. The real (ε') and imaginary parts (ε'') of permittivity are related to the capacitive and dissipative effects in the material[29,41].

The ε' of CX composites (Figure 9a and 9b) are observed between 5.4 and 8.1, while the ε'' had a maximum at approximately 0.5. A rise in ε' is seen when the percentage of CX increased to 15 wt.% in the polymer matrix (Figure 9b). The composites containing CNT 10CX/0.1CNT and 15CX/0.1CNT (Figures 9c and 9d) showed ε' curves between 5.7 and 9.9. The ε'' of the 15CX/0.1CNT sample increased with the frequency variation, reaching a maximum of approximately 1.5. The increase of CX concentration (15 wt.%) associated with the addition of CNT promoted the rise of ε' and ε'', improving the dielectric property. This effect can be attributed to a polarization interface due to the creation of dipoles between the CX interface and the polymer matrix[61,62]. The increase in the ε'', shown in Figure 9d, might be related to an increase in electrical conductivity, probably related to the higher concentration of porous carbon[29,63].

Usually, materials with RL values lower than -10 dB are considered absorbers of EM radiation[45,64]. The 10CX shows a maximum RL of -11.08 dB at 16.72 GHz for a thickness of 5.80 mm (Figure 10a) and a bandwidth of 0.6 GHz. Increasing the percentage of sustainable carbon material on the composite (15CX) improves the attenuation to -13.98 dB

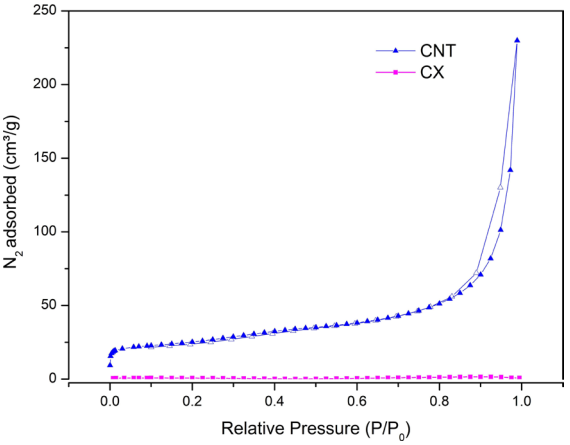

Figure 6. N_2 adsorption-desorption (solid and open symbols, respectively) isotherms of CNT and CX.

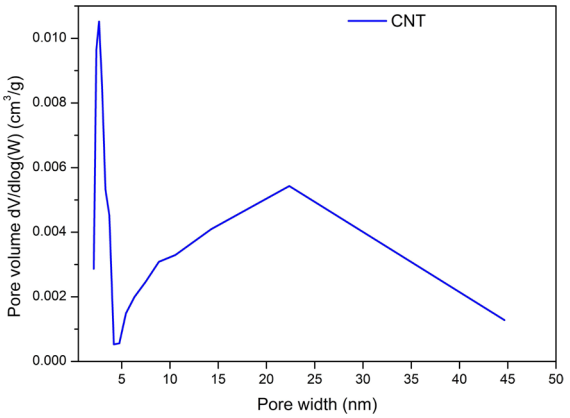

Figure 7. Pore size distribution of CNT.

Table 1. BET surface area (S_{BET}), total pore volume ($V_{total\ 0.99}$), micropore volume (V_{DR}), mesopore volume (V_{meso}).

Sample	S_{BET} ($m^2.g^{-1}$)	$V_{total0.99}$ ($cm^3.g^{-1}$)	V_{DR} ($cm^3.g^{-1}$)	V_{meso} ($cm^3.g^{-1}$)	V_{DR} / $V_{0.99}$ (%)	V_{meso} / $V_{0.99}$ (%)
CNT	90	0.22	0.03	0.19	14	86
CX	3	-	-	-	-	-

at 17.30 GHz for 5.25 mm (Figure 10b). The saturation concentration (15CX) and the increase in material thickness (6.25 mm) promoted a shift to 14.33 GHz with a slight decrease in RL (-15.97 dB), and an increase in bandwidth to approximately 0.9 GHz. The increased concentration of CX from 10 wt.% to 15 wt.% could also raise the number of pores in the composite, improving the attenuation capacity of the EM wave. The 10CX/0.1CNT composite (Figure 10-c) showed a great improvement in RL at -17.70 dB (15.90 GHz) and -20.12 dB (17.95 GHz), respectively in thicknesses of 5.00 mm and 5.90 mm. The bandwidth of the 5.90 mm

Table 2. Bulk density (ρ_b), skeletal density (ρ_s), porosity (ϕ), total pore volume (V_{Hg}), total pore area (A_{total}).

Sample	ρ_b (g.mL^{-1})	ρ_s (g.mL^{-1})	ϕ (%)	V_{Hg} (mL.g^{-1})	A_{total} (m^2.g^{-1})
CX	0.40	0.87	52	1.29	67

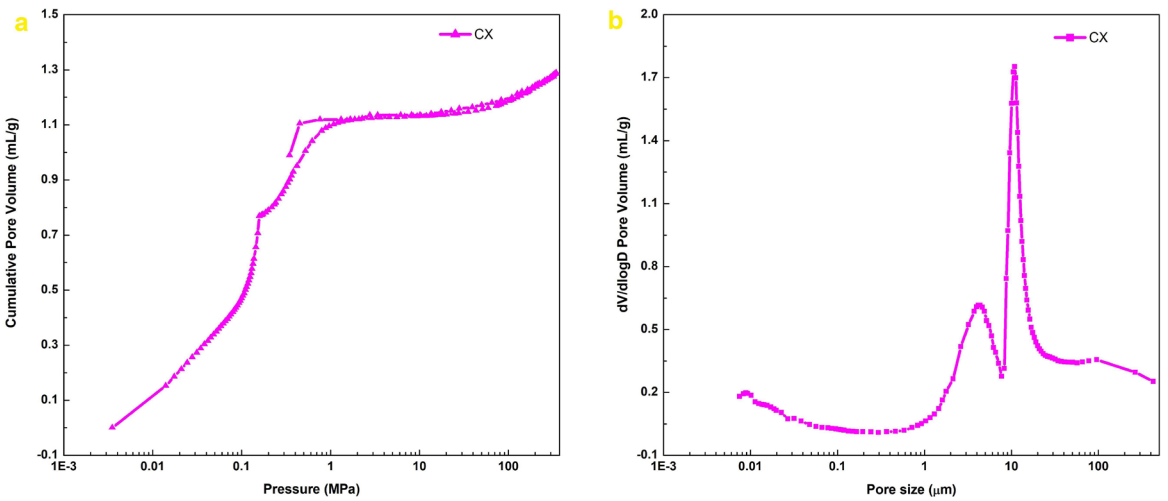

Figure 8. Mercury porosimetry of CX: a) raw intrusion-extrusion curves b) corresponding pore-size distribution.

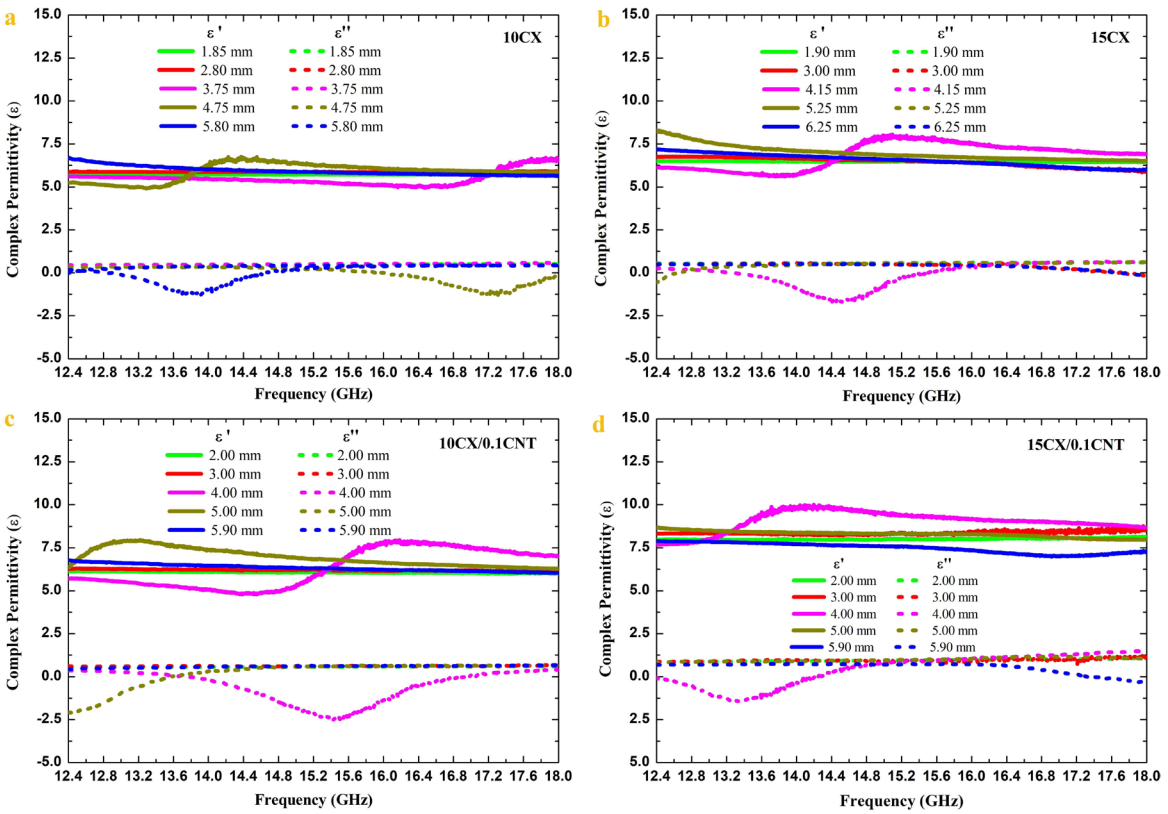

Figure 9. Complex permittivity of composites a) 10CX, b) 15CX, c) 10CX/0.1CNT, d) 15CX/0.1CNT.

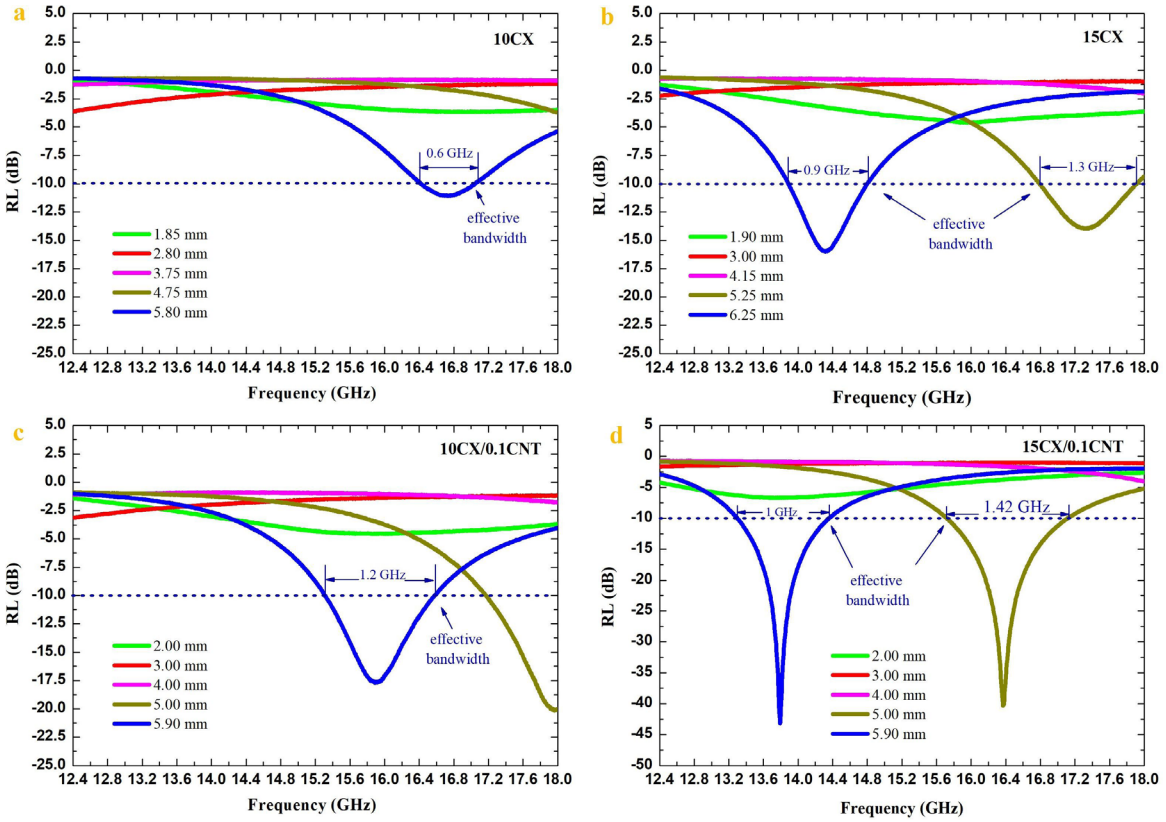

Figure 10. RL of a) 10CX, b) 15CX, c) 10CX/0.1CNT and d) 15CX/0.1CNT composites.

thick sample has been increased to 1.2 GHz. However, with the increasing concentration of sustainable material in the composite, reaching saturation (Figure 10d), a notable rise in RL was observed at -43.19 dB (13.79 GHz) and -40.17 dB (16.36 GHz), referring to the thicknesses of 5.00 mm and 5.90 mm, with a bandwidth of 1.00 and 1.42 GHz, respectively.

As expected, the composites at a higher concentration of CX in the presence of CNT (15CX/0.1CNT) improve the dielectric losses (ε''≅1)[29], which may be associated with the increased attenuation of the EM wave presented in the RL results.

Based on the above discussion, Figure 11 illustrates the possible absorption mechanisms of electromagnetic wave (EW) for the composites. First, when the EW reaches the interior of the samples, multiple reflections can occur. The pores on CX may also contribute to scattering the EW. At this point, the EW energy is transformed and dissipated[16].

Secondly, the CNT has a considerably low specific mass of 0.28 g/cm^3, representing a large volume even at small mass fractions. Thus, inserting only 0.1 wt.% of CNT can significantly increase the number of interfaces between CX/CNT, and the synergic effect between CX and CNT favors the formation of interfacial polarization[65], which would explain the improvement in the RL parameters in the composite. It is also important to notice that heterogeneous interfaces associated with different materials can cause interfacial polarization[66] or Maxwell-Wagner-Sillars effect[67,68]. Besides, the interfacial polarization will be enhanced due to the elevated porosity of

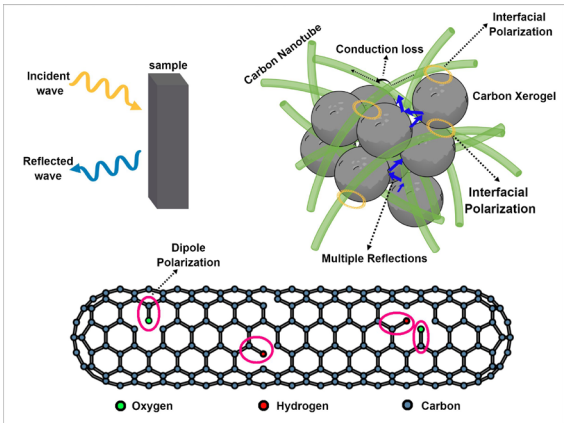

Figure 11. Illustration of the EW absorption mechanisms in the CX/CNT composite.

the CNT and CX. Concurrently, the conduction loss cannot be discarded because the alternating current conductivity increases with ε'' enhancing conduction loss.

Finally, vacancies and lattice defects in the carbon structure contribute to dipole polarization. The defects in CX and CNT will be an additional source of dipole polarization center. The Raman spectra display a D band near 1350 cm^{-1}, corresponding to the disordered structure of amorphous carbon, Figure 4. The D-band presence corroborates the

Table 3. Electromagnetic properties of carbon gels.

Sample	Matrix	Thickness (mm)	RL (dB)	Frequency (GHz)	Reference
15CX/0.1CNT	silicone	5.00	-40.17	16.36	this work
		5.90	-43.19	13.79	
Hollow carbon spheres	paraffin	2.00	-23.35	5.73	Fan et al.[1]
Graphene-CNT Aerogel	paraffin	3.30	-54.00	9.12	Zhu et al.[43]
Carbon Aerogel	PMMA	2.20	-48.00	10.00	Mahani et al.[2]

existence of defects that will become dipole polarization centers[2,16,69]. Thus, the dominant dielectric loss mechanism stems from interfacial polarization, dipole polarization, multiple reflections, and conduction loss[70].

Additionally, the thickness of the CX/CNT composites, when it exceeds 5.00 mm, plays a relevant role in affecting the intensity of the RL[71]. The incident EW cannot be totally absorbed. A significant part of the EW is reflected on the metal plate interface. When the absorber layer thickness is equal to one-quarter electrical wavelength, the incident and reflected waves are 180° out of phase, resulting in a total mutual cancelation at the air-absorber interface. This phenomenon can be explained by the quarter-wavelength matching model. The absorber thickness (t_m) for the cancellation effect can be expressed according to the quarter-wavelength matching model[1,45,64,71-73]:

$$t_m = \frac{\lambda}{4\sqrt{|\varepsilon_r||\mu_r|}} = \frac{nc}{4f_m\sqrt{|\varepsilon_r||\mu_r|}}(n = 1,3,5,\ldots)$$

where t_m is matching thickness, f_m the peak frequency related to the minimum RL value, λ the wavelength of the EW, c the velocity of light, ε_r the complex permittivity and μ_r the complex permeability of the microwave absorber.

Figure 12 shows the relationship between the absorber thickness and the more intense RL peaks of the 15CX/0.1CNT sample, where the black line refers to a 3λ/4 plot. Therefore, the t_m values are evidently consistent with the effect of quarter wavelength (λ/4) cancellation, corresponding to a minimum RL value. The RL curves of the most intense peaks of the 15CX0.1CNT composite show that the peak position changes to a lower frequency as the thickness increases from 5.00 to 5.90 mm, following the rule of variation of the absorption peak with the thickness and frequency, indicating that the attenuation of the EW by microwaves can also include the contribution of absorption and destructive interference[74,75].

Table 3 shows that the characteristics of the sustainable composite are comparable to carbon aerogels from synthetic phenolic sources. The CX composite is among the materials with the highest absorption capacity (99.99%) and presents a slight difference from the composite with the highest absorbing potential, Graphene-CNT Aerogel (99.999%)[43]. However, the CX produced in this work is synthesized from a natural phenolic using a simple synthesis route, that is, dried under ambient temperature and pressure, resulting in a sustainable and low-cost composite, while the other materials were synthesized using more expensive synthetic products, in addition to synthesis routes with extensive stages, including the supercritical drying, increasing the cost of the final product.

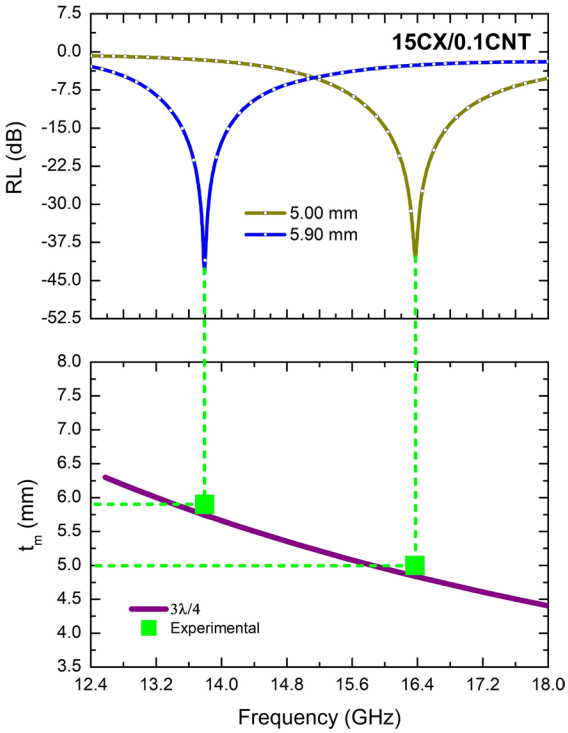

Figure 12. Relationship between the RL peaks frequency and calculated thickness of 15CX/0.1CNT.

Therefore, the sustainable composite 15CX/0.1CNT has relevant characteristics such as RAM. The mixture of sustainable CX with CNT probably promoted the pathway network on the material's surface, improving the absorption performance and quarter-wave matching. Additionally, the porosity of the material can also contribute to the attenuation due to multiple reflections and wave scattering that may occur within pores, therefore increasing the absorption capacity[1,2,14,43].

4. Conclusions

This paper demonstrates an alternative route to producing sustainable, flexible, low density, and low-cost composites in the production of RAM. CX was synthesized from a natural polyphenolic, tannin, replacing synthetic phenolics such as resorcinol and phenol. The increase in the concentration of porous CX without adding CNT in the polymer matrix favored an increase in RL intensity, reaching values over 90% of absorption of the EW. The sustainable 15CX/0.1CNT composite showed EW absorption properties, resulting in an

RL of -43.19 dB, representing an attenuation of 99.99% at 13.79 GHz. The microwave absorption properties may be improved by adjusting the amount of CNT in the composite. The EM properties demonstrated that a composite using sustainable porous carbon is a strong candidate for the development of sustainable RAM composites.

5. Acknowledgments

This work has been supported by the following Brazilian research agencies: Coordenação de Aperfeiçoamento de Pessoal Nível Superior – Brasil (CAPES) – Finance Code 001, Financiadora de Estudos e Projetos (FINEP) and Conselho Nacional de Desenvolvimento Científico e Tecnológico (CNPq). The authors Nila Cecília de Faria Lopes Medeiros and Leonardo Iusuti de Medeiros thank Universidade Estadual de Santa Cruz (UESC) and Instituto Nacional de Pesquisas Espaciais (INPE).

6. References

1. Fan D, Wei B, Wu R, Zhou J, Zhou C. Dielectric control of ultralight hollow porous carbon spheres and excellent microwave absorbing properties. J Mater Sci. 2021;56(11):6830-44.
2. Mahani AA, Motahari S, Nayyeri V. Electromagnetic and microwave absorption characteristics of PMMA composites filled with a nanoporous resorcinol formaldehyde based carbon aerogel. RSC Advances. 2018;8(20):10855-64.
3. Wang J, Zhou M, Xie Z, Hao X, Tang S, Wang J, et al. Enhanced interfacial polarization of biomass-derived porous carbon with a low radar cross-section. J Colloid Interface Sci. 2022;612:146-55.
4. Allam Z, Sharifi A, Giurco D, Sharpe SA. Green new deals could be the answer to COP26's deep decarbonisation needs. Sustainable Horizons. 2022;1:100006.
5. Pizzi A, Khan A, Asiri AM. Wood bioadhesives for biocomposites by nonvolatile bioaldehydes generation by specific oxidation of different biomaterials. In: Khan A, Jawaid M, Pizzi A, Azum N, Asiri A, Isa I, editors. Advanced technology for the conversion of waste into fuels and chemicals. Cham: Elsevier; 2021. p. 449-66. http://dx.doi.org/10.1016/B978-0-12-823139-5.00017-4.
6. Pizzi A. Tannins: prospectives and actual industrial applications. Biomolecules. 2019;9(8):1-30.
7. Braghiroli FL, Amaral-Labat G, Boss AFN, Lacoste C, Pizzi A. Tannin gels and their carbon derivatives: a review. Biomolecules. 2019;9(10):587.
8. Shirmohammadli Y, Efhamisisi D, Pizzi A. Tannins as a sustainable raw material for green chemistry: a review. Ind Crops Prod. 2018;126:316-32.
9. Amaral-Labat G, Szczurek A, Fierro V, Pizzi A, Celzard A. Systematic studies of tannin-formaldehyde aerogels: preparation and properties. Sci Technol Adv Mater. 2013;14(1):1-13.
10. Szczurek A, Amaral-Labat G, Fierro V, Pizzi A, Masson E, Celzard A. The use of tannin to prepare carbon gels. Part I: carbon aerogels. Carbon. 2011;49(8):2773-84.
11. Amaral-Labat G, Grishechko LI, Fierro V, Kuznetsov BN, Pizzi A, Celzard A. Tannin-based xerogels with distinctive porous structures. Biomass Bioenergy. 2013;56:437-45.
12. Amaral-Labat G, Szczurek A, Fierro V, Celzard A. Unique bimodal carbon xerogels from soft templating of tannin. Mater Chem Phys. 2015;149:193-201.
13. Amaral-Labat G, Munhoz MGC, Fonseca BCS, Boss AFN, de Almeida-Mattos P, Braghiroli FL, et al. Xerogel-like materials from sustainable sources: properties and electrochemical performances. Energies. 2021;14(23):7977.
14. Castro-Gutiérrez J, Palaimiene E, Macutkevic J, Banys J, Kuzhir P, Schaefer S, et al. Electromagnetic properties of carbon gels. Materials. 2019;12(24):1-9.
15. Song WL, Cao M-S, Fan L-Z, Lu M-M, Li Y, Wang C-Y, et al. Highly ordered porous carbon/wax composites for effective electromagnetic attenuation and shielding. Carbon. 2014;77:130-42. http://dx.doi.org/10.1016/j.carbon.2014.05.014.
16. Tao J, Zhou J, Yao Z, Jiao Z, Wei B, Tan R, et al. Multi-shell hollow porous carbon nanoparticles with excellent microwave absorption properties. Carbon. 2021;172:542-55.
17. Gupta S, Tai N. Carbon materials and their composites for electromagnetic interference shielding effectiveness in X-band. Carbon. 2019;152:159-87.
18. Drakakis E, Kymakis E, Tzagkarakis G, Louloudakis D, Katharakis M, Kenanakis G, et al. A study of the electromagnetic shielding mechanisms in the GHz frequency range of graphene based composite layers. Appl Surf Sci. 2017;398:15-8.
19. Ruiz-Perez F, López-Estrada SM, Tolentino-Hernández RV, Caballero-Briones F. Carbon-based radar absorbing materials: a critical review. J Sci Adv Mater Dev. 2022;7:100454.
20. Ning M, Li J, Kuang B, Wang C, Su D, Zhao Y, et al. One-step fabrication of N-doped CNTs encapsulating M nanoparticles (M = Fe, Co, Ni) for efficient microwave absorption. Appl Surf Sci. 2018;447:244-53.
21. Raveendran A, Sebastian MT, Raman S. Applications of microwave materials: a review. J Electron Mater. 2019;48(5):2601-34. http://dx.doi.org/10.1007/s11664-019-07049-1.
22. Jinxiao W, Jianfeng Y, Jun Y, Hui Z. Design of a novel carbon nanotube and metal-organic framework interpenetrated structure with enhanced microwave absorption properties. Nanotechnology. 2020;31(39):394002.
23. Zhang Z, Cai Z, Wang Z, Peng Y, Xia L, Ma S, et al. A review on metal-organic framework-derived porous carbon-based novel microwave absorption materials. Nano-Micro Lett. 2021;13(1):56.
24. Chung DDL, Xi X. Factors that govern the electric permittivity of carbon materials in the graphite allotrope family. Carbon. 2021;184:245-52.
25. Green M, Chen X. Recent progress of nanomaterials for microwave absorption. Journal of Materiomics. 2019;5(4):503-41.
26. Yang S, Sun X, Wang S, Ning Y, Yuan Y, Yin W, et al. Electromagnetic wave absorbing properties of coconut shell-derived nanocomposite. Carbon. 2022;196:354-64.
27. Wang Y-L, Yang S-H, Wang H-Y, Wang G-S, Sun X-B, Yin P-G. Hollow porous CoNi/C composite nanomaterials derived from MOFs for efficient and lightweight electromagnetic wave absorber. Carbon. 2020;167:485-94..
28. Bispo MC, Lopes BHK, Fonseca BCS, Portes RC, Matsushima JT, Yassuda MKH, et al. Electromagnetic properties of carbon-graphene xerogel, graphite and ni-zn ferrite composites in polystyrene matrix in the x-band (8.2-12.4 GHz). Materia (Rio J). 2021;26(2):e12967.
29. Flórez Vergara DE, Lopes BHK, Quirino SF, Silva GFBL, Boss AFN, Amaral-Labat GA, et al. Frequency selective surface properties of microwave new absorbing porous carbon materials embedded in epoxy resin. Mater Res. 2019;22(Suppl. 1):e20180834.
30. Inagaki M, Qiu J, Guo Q. Carbon foam: preparation and application. Carbon. 2015;87:128-52.
31. Kuzhir PP, Paddubskaya AG, Maksimenko SA, Celzard A, Fierro V, Amaral-Labat G, et al. Highly porous conducting carbon foams for electromagnetic applications. In: IEEE International Symposium on Electromagnetic Compatibility; 2012; Rome, Italy. Proceedings. New York: IEEE; 2012. p. 1-4. http://dx.doi.org/10.1109/EMCEurope.2012.6396811.
32. Kuzhir PP, Paddubskaya AG, Shuba MV, Maksimenko SA, Celzard A, Fierro V, et al. Electromagnetic shielding efficiency

in Ka-band: carbon foam versus epoxy/carbon nanotube composites. J Nanophotonics. 2012;6(1):061715.
33. Jayalakshmi CG, Inamdar A, Anand A, Kandasubramanian B. Polymer matrix composites as broadband radar absorbing structures for stealth aircrafts. J Appl Polym Sci. 2019;136:1-21.
34. IEEE: Institute of Electrical and Electronics Engineers. IEEE standard letter designations for radar-frequency bands. New York: IEEE; 2003. 10 p. http://dx.doi.org/10.1109/IEEESTD.2003.94224.
35. Fakharian MM, Alibakhshikenari M, See CH, Abd-Alhameed R. A high gain multiband offset MIMO antenna based on a planar log-periodic array for Ku/K-band applications. Sci Rep. 2022;12(1):1-13.
36. Guo J, Wu H, Liao X, Shi B. Facile synthesis of size-controlled silver nanoparticles using plant tannin grafted collagen fiber as reductant and stabilizer for microwave absorption application in the whole Ku band. J Phys Chem C. 2011;115(48):23688-94.
37. Chen N, Wang X-Y, Li D, Jiang J-T, Guan Z-J, Wang K-J. Constructing and optimizing core-shell structured Co@TiO2 as highly efficient electromagnetic wave absorber. J Mater Sci Mater Electron. 2021;32(23):27636-46.
38. Barde C, Choubey A, Sinha R, Mahto SK, Ranjan P. A compact wideband metamaterial absorber for Ku band applications. J Mater Sci Mater Electron. 2020;31(19):16898-906.
39. Brunauer S, Emmett PH, Teller E. Adsorption of gases in multimolecular layers. J Am Chem Soc. 1938;60(2):309-19.
40. Dubinin MM. Fundamentals of the theory of adsorption in micropores of carbon adsorbents: characteristics of their adsorption properties and microporous structures. Carbon. 1989;27(3):457-67.
41. Souza AAT, Medeiros NCFL, Medeiros LI, Amaral-Labat GA, Bispo MC, Lenz e Silva GFB, et al. Double layer material designed to reduce electromagnetic radiation with carbon black, silicon carbide and manganese zinc ferrite. J Aerosp Technol Manag. 2021;13:1-12.
42. Medeiros NCFL, Medeiros LI, Souza AAT, Silva GFBL, Boss AFN, Amaral-Labat GA, et al. Electromagnetic characterization of the silicon carbide and carbon black composite in a polymeric matrix. Materia. 2021;26:e12971.
43. Zhu Y, Guan X, Yang Z. One-pot synthesis of carbon nanotube reinforced graphene aerogels and their applications in electromagnetic wave attenuation. J Phys Chem Solids. 2021;159:110279. http://dx.doi.org/10.1016/j.jpcs.2021.110279.
44. Muzyka R, Drewniak S, Pustelny T, Chrubasik M, Gryglewicz G. Characterization of graphite oxide and reduced graphene oxide obtained from different graphite precursors and oxidized by different methods using Raman spectroscopy. Materials. 2018;11(7):15-7.
45. Jiang Y, Fu X, Zhang Z, Fan G, Liu Y, Du W, et al. Chiffon cake-derived hierarchically porous carbon with efficient microwave absorption properties. J Mater Sci Mater Electron. 2019;30(21):19173-81.
46. Hirschmann TC, Dresselhaus MS, Muramatsu H, Seifert M, Wurstbauer U, Parzinger E, et al. G'Band in double- and triple-walled carbon nanotubes: a Raman study. Phys Rev B Condens Matter Mater Phys. 2015;91(7):1-9.
47. DiLeo RA, Landi BJ, Raffaelle RP. Purity assessment of multiwalled carbon nanotubes by Raman spectroscopy. J Appl Phys. 2007;101(6):064307.
48. Jorio A, Saito R. Raman spectroscopy for carbon nanotube applications. J Appl Phys. 2021;129(2):021102.
49. Pimenta MA, Dresselhaus G, Dresselhaus MS, Cançado LG, Jorio A, Saito R. Studying disorder in graphite-based systems by Raman spectroscopy. Phys Chem Chem Phys. 2007;9(11):1276-91.
50. Habeb Abdulrazzak F, Fadel Alkiam A, Hasan Hussein F. Behavior of X-ray analysis of carbon nanotubes. In: Saleh HM, El-Sheikh SMM, editors. Perspective of carbon nanotubes. London: IntechOpen; 2019. http://dx.doi.org/10.5772/intechopen.85156.
51. Giri PK, Singh DK. Possible role of defects in the visible photoluminescence from single walled and multiwalled carbon nanotubes. Mater Res Soc Symp Proc. 2007;1018:93-8.
52. Soleimani H, Yahya N, Baig MK, Khodapanah L, Sabet M, Burda M, et al. Synthesis of carbon nanotubes for oil-water interfacial tension reduction. Oil Gas Res. 2015;1:1.
53. Yue X, Arenillas A, Irvine JTS. Application of infiltrated LSCM-GDC oxide anode in direct carbon/coal fuel cells. Faraday Discuss. 2016;190:269-89.
54. Fathi Z, Khavari Nejad RA, Mahmoodzadeh H, Satari TN. Investigating of a wide range of concentrations of multi-walled carbon nanotubes on germination and growth of castor seeds (*Ricinus communis* L.). J Plant Prot Res. 2017;57(3):228-36.
55. Alegre C, Sebastián D, Lázaro MJ. Carbon xerogels electrochemical oxidation and correlation with their physico-chemical properties. Carbon. 2019;144:382-94.
56. Celzard A, Fierro V, Amaral-Labat G. Adsorption by carbon gels. In: Tascon JMDB, editor. Novel carbon adsorbents. Amsterdam: Elsevier; 2012. p. 207-44. http://dx.doi.org/10.1016/B978-0-08-097744-7.00007-7.
57. Thommes M, Kaneko K, Neimark AV, Olivier JP, Rodriguez-Reinoso F, Rouquerol J, et al. Physisorption of gases, with special reference to the evaluation of surface area and pore size distribution (IUPAC Technical Report). Pure Appl Chem. 2015;87(9-10):1051-69.
58. Bardestani R, Patience GS, Kaliaguine S. Experimental methods in chemical engineering: specific surface area and pore size distribution measurements—BET, BJH, and DFT. Can J Chem Eng. 2019;97(11):2781-91.
59. Barrett EP, Joyner LG, Halenda PP. The determination of pore volume and area distributions in porous substances. i. computations from nitrogen isotherms. J Am Chem Soc. 1951;73(1):373-80.
60. Wang J, Huyan Y, Yang Z, Zhang A, Zhang Q, Zhang B. Tubular carbon nanofibers: synthesis, characterization and applications in microwave absorption. Carbon. 2019;152:255-66.
61. Sriramulu G, Maramu N, Reddy BR, Kandasami A, Katlakunta S. Structural, magnetic and electromagnetic properties of microwave-hydrothermally synthesized $Sr(Zr\text{-}Mn)_{2x}Fe_{12\text{-}2x}O_{19}$ hexaferrites. Mater Res Bull. 2022;149:111732.
62. Kiani E, Rozatian ASH, Yousefi MH. The effects of doping on crystal structure, magnetic and microwave properties of $SrFe_{12\text{-}2x}$ La x $(Mn_{0.5}Zr_{0.5})_x$ O_{19} nanoparticles. J Supercond Nov Magn. 2013;26(3):733-8.
63. Szczurek A, Fierro V, Plyushch A, Macutkevic J, Kuzhir P, Celzard A. Structure and electromagnetic properties of cellular glassy carbon monoliths with controlled cell size. Materials. 2018;11(5):709.
64. Li G, Wang L, Li W, Ding R, Xu Y. $CoFe_2O_4$ and/or Co_3Fe_7 loaded porous activated carbon balls as a lightweight microwave absorbent. Phys Chem Chem Phys. 2014;16(24):12385-92.
65. Zhang Z, Zhao Y, Li Z, Zhang L, Liu Z, Long Z, et al. Synthesis of carbon/SiO_2 core-sheath nanofibers with Co-Fe nanoparticles embedded in via electrospinning for high-performance microwave absorption. Adv Compos Hybrid Mater. 2022;5(1):513-24.
66. Yan L, Hong C, Sun B, Zhao G, Cheng Y, Dong S, et al. In situ growth of core-sheath heterostructural SiC nanowire arrays on carbon fibers and enhanced electromagnetic wave absorption performance. ACS Appl Mater Interfaces. 2017;9(7):6320-31.
67. Liu L, He N, Wu T, Hu P, Tong G. Co/C/Fe/C hierarchical flowers with strawberry-like surface as surface plasmon for enhanced permittivity, permeability, and microwave absorption properties. Chem Eng J. 2019;355:103-8.
68. He S, Lu C, Wang G-S, Wang J-W, Guo H-Y, Guo L. Synthesis and growth mechanism of white-fungus-like nickel sulfide microspheres, and their application in polymer composites with

enhanced microwave-absorption properties. ChemPlusChem. 2014;79(4):569-76.
69. Zong Z, Ren P, Guo Z, Wang J, Chen Z, Jin Y, et al. Three-dimensional macroporous hybrid carbon aerogel with heterogeneous structure derived from MXene/cellulose aerogel for absorption-dominant electromagnetic interference shielding and excellent thermal insulation performance. J Colloid Interface Sci. 2022;619:96-105.
70. Biswas S, Arief I, Panja SS, Bose S. Absorption-dominated electromagnetic wave suppressor derived from ferrite-doped cross-linked graphene framework and conducting carbon. ACS Appl Mater Interfaces. 2017;9(3):3030-9.
71. Gupta S, Tai NH. Carbon materials and their composites for electromagnetic interference shielding effectiveness in X-band. Carbon. 2019;152:159-87.
72. Huang X, Zhang J, Lai M, Sang T. Preparation and microwave absorption mechanisms of the NiZn ferrite nanofibers. J Alloys Compd. 2015;627:367-73.
73. Bora PJ, Azeem I, Vinoy KJ, Ramamurthy PC, Madras G. Morphology controllable microwave absorption property of polyvinylbutyral (PVB)-MnO_2 nanocomposites. Compos, Part B Eng. 2018;132:188-96.
74. Lei L, Yao Z, Zhou J, Wei B, Fan H. 3D printing of carbon black/polypropylene composites with excellent microwave absorption performance. Compos Sci Technol. 2020;200:108479.
75. Shen Y, Zhang F, Song P, Zhang Y, Zhang T, Wen X, et al. Design and synthesis of magnetic porous carbon nanofibers with excellent microwave absorption. J Alloys Compd. 2022;903:163971.